Effect of ambipolar fluxes on nanoparticle charging in low-pressure glow discharges

K. Ostrikov*
School of Physics, The University of Sydney, Sydney, New South Wales 2006, Australia
(Received 15 July 2004; revised manuscript received 10 September 2004; published 14 February 2005)

The effect of ambipolar fluxes on nanoparticle charging in a typical low-pressure parallel-plate glow discharge is considered. It is shown that the equilibrium values of the nanoparticle charge in the plasma bulk and near-electrode areas are strongly affected by the ratio ς_{ath}^{i} of the ambipolar flux and the ion thermal velocities. Under typical experimental conditions the above ratio is neither $\varsigma_{ath}^{i} \ll 1$ nor $\varsigma_{ath}^{i} \gg 1$, which often renders the commonly used approximations of the purely thermal or "ion wind" ion charging currents inaccurate. By using the general approximation for the ambipolar drift-affected ion flux on the nanoparticle surface, it appears possible to obtain more accurate values of the nanoparticle charge that usually deviate within 10–25 % from the values obtained without a proper accounting for the ambipolar ion fluxes. The implications of the results obtained for glow discharge modeling and nanoparticle manipulation in low-pressure plasmas are discussed.

DOI: 10.1103/PhysRevE.71.026405 PACS number(s): 52.25.Vy, 52.27.Lw, 52.80.−s

I. INTRODUCTION

Management of fine powder particles generated in low-temperature processing plasmas remains one of the major problems for the development of new dust-free process cycles in the semiconductor microchip manufacturing and, more recently, for the plasma-assisted structural nanoparticle incorporation-based fabrication of advanced nano- and biomaterials and devices [1–4]. In this regard, the shape, elemental and structural composition, and transport properties of the fine particles are among the most critical issues in the achievement of greater predictability and control of future industrial processes involving nanosized clusters and particulates as building units of various nanoassemblies [5–7]. In ionized gas environments the nanoparticle transport properties are mostly controlled by long-range interactions that critically depend on the particle charge [7]. To this end, the problem of nanoparticle manipulation in the plasma does require a great precision in the diagnostics and management of its equilibrium charge and charge fluctuations in low-pressure glow discharges.

Extensive research efforts have been focused in the last decade on the modeling of discharge parameters and fine particle nucleation and charging. Among various existing discharge configurations, parallel-plate discharges remain one of the most popular discharge geometries owing to their cost efficiency, simplicity in operation, and widespread applications in industry [8]. Some of these efforts include modeling of diffusion equilibria, spatial profiles of the main plasma parameters, charge fluctuations, and clustering processes (see, e.g., Refs. [9–12] and references therein).

In the modeling of "dusty" gas discharges (where the solid particles can either nucleate in the gas phase or be externally introduced to the plasma) the details of particle charging are indispensable for the accurate description of the particle and power balance processes. The charging processes are affected by two groups of factors. The "internal" factors include, e.g., the particle shape, composition, and size, whereas the "external" factors are mostly related to the microscopic electron and ion charging currents driven in the plasma discharge. For example, a distinctive feature of the parallel-plate glow discharges of our interest here is a clear one-dimensional geometry, wherein the electron and ion loss to the parallel-plate electrodes is controlled by ambipolar fluxes that originate due to intrinsic nonuniformities of the discharge plasma and the tendency of the plasma to maintain its quasineutrality throughout the entire discharge volume, excluding the near-electrode sheath areas [13,14].

While the nonuniformity of the plasma parameters and ambipolar fluxes has been routinely included in numerous numerical models of the electron and ion and power balance in "dusty" discharges, the effect of the ambipolar fluxes on fine particle charging has not attracted the attention it merits, despite recent encouraging reports that the dust component can act as a charge sink and significantly affect the ambipolar diffusion scale length [15,16]. Indeed, the most commonly used approach to calculate the dust charge in the plasma bulk is based on the assumption of the purely thermal (and hence, spherically symmetrical) ion charging current

$$I_i = e\pi a_p^2 V_{Ti} n_i (1 - e\Delta_{ps}/T_i), \tag{1}$$

where $\Delta_{ps} = \phi_p - \phi_s$ is the difference between the particle surface ϕ_s and the ambient plasma ϕ_p potentials, a_p is the particle radius, and n_i, T_i, $V_{Ti} = (2T_i/m_i)^{1/2}$, and m_i are the ion density, temperature, thermal velocity, and mass, respectively [17–19]. This approach requires that the directed ion flux with velocity v_{iD} is strongly subthermal ($v_{iD} \ll V_{Ti}$). This assumption is undoubtedly correct in situations when there are no physical means, such as any appreciable electric fields, to sustain directed ion fluxes. For example, in "ideal" plasma bulk areas, the electrostatic potential and electron and ion densities are assumed uniform, which effectively eliminates any noticeable directed ion flows [20]. On the other hand, in

*Also with Plasma Sources and Applications Center, NIE, Nanyang Technological University, 637616 Singapore.
Electronic address: K.Ostrikov@physics.usyd.edu.au

the near-electrode sheath areas, the ion flux is usually superthermal, and the "ion wind" approximation

$$I_i = e\pi a_p^2 v_{iD} n_i (1 - 2e\Delta_{ps}/m_i v_{iD}^2) \quad (2)$$

for the microscopic ion current is commonly used when $v_{iD} \gg V_{Ti}$ [17,18].

In most common glow discharges that feature nonuniform plasma density distributions, from fairly uniform in the plasma bulk to strongly nonuniform (and also non-neutral) in the plasma sheaths, the physical conditions for dust charging change dramatically when the particle is moved along the plasma nonuniformity. Indeed, in the plasma bulk without any significant directed ion fluxes, Eq. (1) is a fair approximation, whereas Eq. (2) would be more appropriate for the near-electrode areas. To accommodate a continuous change of the ion velocity from V_{Ti} (in the plasma bulk) to v_{iD} (which exceeds the Bohm velocity in the plasma sheath) in a single formula, it is very common to use Eq. (2) in all discharge areas with v_{iD} replaced by the mean ion velocity $v_i = [(v_{iD})^2 + V_{Ti}^2]^{1/2}$. However, this approach can easily fail in the discharge areas (e.g., in the presheath) where the directed ion velocity is comparable with (or even higher than) V_{Ti}, and a general expression for the microscopic ion charging current [21], valid at arbitrary values of the ratio $s_{ath}^i = v_{iD}/V_{Ti}$, should be used instead of the simplified expressions (1) and (2).

Furthermore, under certain conditions the ambipolar electric fields and, hence, directed fluxes of the plasma species are appreciable even in the plasma bulk, which is usually sidestepped in many existing models of dust-contaminated discharges. The relative importance of the directed and thermal ion velocities in the microscopic ion charging current depends on many factors such as the width of the plasma slab, collision rates, actual plasma nonuniformity, electron and ion temperatures, and some others. Here, we explore situations when the speed of directed ion fluxes originating due to the ambipolar electric fields in nonuniform plasmas exceeds the ion thermal velocity and significantly affects the nanoparticle charging process by modifying the microscopic ion charging currents. By using the general approximation for the ambipolar drift-affected ion flux on the nanoparticle surface, we numerically obtain more accurate values of the nanoparticle charge and discuss the implications of the results obtained for glow discharge modeling and nanoparticle manipulation in low-pressure plasmas.

II. FORMULATION AND MAIN EQUATIONS

A schematic diagram of the parallel-plate discharge configuration of our interest here is shown in Fig. 1. To illustrate the effect of ambipolar fluxes on the equilibrium nanoparticle charge, a simple discharge model has been adopted. Two large-area elecrodes are separated by the interelectrode spacing L, which is assumed to be much less than the linear dimensions of the electrodes in the y and z directions and much larger than the mean free path of the plasma species. The number densities of electrons and ions are nonuniform along the x direction, whereas the electron and ion temperatures are assumed uniform in the plasma slab. Solid spherical

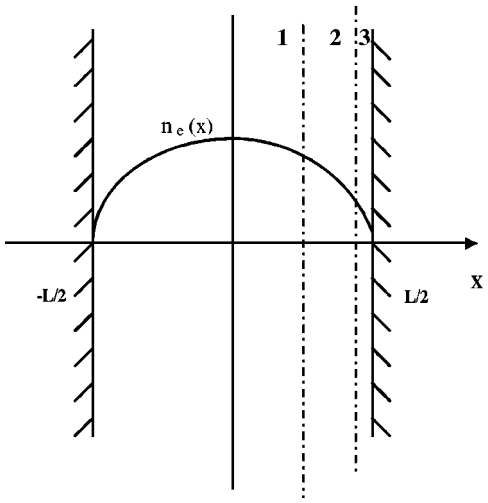

FIG. 1. Schematics of the parallel-plate discharge and nonuniform plasma density distribution. 1–3 label the discharge areas with different degrees of plasma nonuniformity.

nanoparticles of the radius a_p and number density n_p uniformly fill the gap between the electrodes. The particle size, which is 10–100 nm [22] in our computations, is smaller than the plasma Debye length λ_D and the mean free path of the plasma species in the electron- and ion-neutral collisions. Any specific details of the particle and power balance required for the study of discharge maintenance, as well as any near-electrode effects, are neglected. It is further assumed that the argon plasma is overall charge neutral and contains singly charged ions Ar^+, electrons, and fine particles. The imbalance between the spatially nonuniform electron $n_e(x)$ and ion $n_i(x)$ number densities is determined from the one-dimensional Poisson equation

$$n_i(x) - n_e(x) - n_p|Z_d(x)| = -(1/4\pi e)\partial^2\phi(x)/\partial x^2, \quad (3)$$

where $Z_d(x)$ is the equilibrium nanoparticle charge and $\phi(x)$ is the plasma potential. At the edges of the plasma slab $x = \pm L/2$, the electron and ion densities vanish, $n_{e,i}(x = \pm L/2) = 0$.

The fluxes of the plasma species $\Gamma_j = n_j v_j$ can be obtained from the steady-state electron and ion balance equations

$$\partial\Gamma_e/\partial x = \nu_i n_e - \nu_{ed} n_e \quad (4)$$

and

$$\partial\Gamma_i/\partial x = \nu_i n_e - \nu_{id} n_i, \quad (5)$$

where it was assumed that the discharge is in the ambipolar diffusion-loss controlled regime, ν_i is the ionization rate, and ν_{id} and ν_{ed} are the rates of electron and ion collection by the fine particles, respectively [23,24]. Here,

$$\Gamma_e = -\mu_e n_e E - D_e(\partial n_e/\partial x) \quad (6)$$

and

$$\Gamma_i = \mu_i n_i E - D_i(\partial n_i/\partial x) \quad (7)$$

are the equilibrium fluxes of the plasma species to the discharge walls, where $D_j = T_j/m_j\nu_{jn}$, $\mu_j = e/m_j\nu_{jn}$, T_j, and m_j

TABLE I. The main plasma and fine particle parameters in the computation.

Parameter	Notation	Value
Electron temperature	T_e	1.0–10.0 eV
Particle size	a_p	10–100 nm
Ion number density ($x=0$)	n_i	8×10^{9}–6×10^{11} cm^{-3}
Electron density ($x=0$)	n_e	6×10^{9}–4×10^{11} cm^{-3}
Particulate density	n_p	2×10^{6}–3×10^{7} cm^{-3}
Positive ion mass (Ar^+)	m_i	$1836\times40\times m_e$
Positive ion temperature	T_i	0.027–0.3 eV
Temperature of neutrals	T_n	0.026 eV
Gas temperature	T_g	20–400 °C
Interelectrode spacing	L	1.0–10.0 cm
Working gas pressure	p_0	5–100 mTorr
Cross section of electron-neutral collisions	σ_{en}	1.5×10^{-15}–5×10^{-15} cm^2
Cross section of ion-neutral collisions	σ_{in}	2×10^{-15}–6×10^{-14} cm^2

are the diffusion and mobility coefficients, temperatures, and masses of the species $j=e,i$, respectively. The rates of the electron- and ion-neutral collisions are $\nu_{en}=N_nV_{Te}\sigma_{en}$ and $\nu_{in}=N_nv_i\sigma_{in}$, respectively. Here, $V_{Te}=(2T_e/m_e)^{1/2}$ is the electron thermal speed, N_n is the density of neutrals, and σ_{en} and σ_{in} are the cross sections of the electron- and ion-neutral collisions.

The ambipolar electric field

$$E_{\mathrm{amb}} = D_i\chi^{-1}\,\partial n_i/\partial x - D_e\chi^{-1}\,\partial n_e/\partial x \tag{8}$$

in the nanoparticle-loaded discharge can be derived from Eqs. (6) and (7) by assuming the ambipolarity of the electron and ion fluxes to the discharge walls $\Gamma_e=\Gamma_i$, where $\chi=\mu_in_i+\mu_en_e$.

The equilibrium electrostatic charge of the (negatively charged) fine particles is calculated by equating the microscopic electron [17,18]

$$I_e = e\pi a_p^2V_{Te}n_e\exp(-e\Delta_{ps}/T_e) \tag{9}$$

and ion [21,25]

$$I_i = \sqrt{\frac{\pi}{2}}a_p^2V_{Ti}en_i\left[2\exp\left(-\frac{v_{iD}^2}{4V_{Ti}^2}\right) + 2\sqrt{\pi}\frac{v_{iD}}{V_{Ti}}\left(1+\frac{v_{iD}^2}{2V_{Ti}^2}-\frac{e\Delta_{ps}}{m_iV_{Ti}^2}\right)\mathrm{erf}\left(\frac{v_{iD}}{2V_{Ti}}\right)\right] \tag{10}$$

charging currents, where $\mathrm{erf}(x)$ is the error function.

III. NUMERICAL RESULTS

In this section, we numerically investigate the effect of the plasma density gradient, electron- and ion-neutral collisions, and nonisothermality of the plasma on the ambipolar fluxes and nanoparticle charge in different areas of the discharge. We begin with a brief discussion of the procedure of calculations and main parameters of the plasma and the fine particles.

A. Procedure and parameter ranges

To illustrate the effect of the ambipolar fluxes on the nanoparticle charging, Eqs. (3)–(10) were solved numerically for the typical parameteres of low-pressure parallel-plate rf discharges shown in Table I. The actual values of ion speed v_{iD}, ion current I_i, and fine particle charge Z_d were compared with the approximate values obtained without accounting for the ambipolar electric field and ion fluxes. The comparison was performed in three distinctive spatial areas of the discharge labeled 1, 2, and 3 in Fig. 1. These areas differ by the degree of nonuniformity of the plasma density, the weakest being in the central discharge area (1 in Fig. 1), and the strongest being in the near-electrode area (3 in Fig. 1). The widths of the areas were varied in the computations to ensure that the minimum difference of the spatially averaged gradient of the plasma density

$$\left\langle\frac{\partial n_{e,i}}{\partial x}\right\rangle = (l_{jr}-l_{jl})^{-1}\int_{l_{jr}}^{l_{jl}}\frac{\partial n_{e,i}}{\partial x}dx$$

in different areas is significant, where l_{jr} and l_{jl} are the right and left boundaries of the jth area. The typical locations of the right borders of the areas 1 and 2 were in the range $l_{1r}\sim(0.5\text{–}0.6)(L/2)$ and $l_{2r}\sim(L/2)-(1\text{–}2.5)\lambda_{mfp}^i$, respectively, where $\lambda_{mfp}^i=v_i/\nu_{in}$ is the mean free path of ions in ion-neutral collisions. Physically, region 1 represents the plasma bulk with weakly nonuniform profiles of the plasma density, region 2 is the area of moderate nonuniformities, and the third area is comparable to a typical presheath primarily responsible for the ion acceleration [26].

Table I summarizes the main parameters used in the computations, which are typical of experiments with nanoparticle-loaded complex ("dusty") plasmas [27]. The specific parameters of the plasma and nanoparticles were chosen within the ranges of validity of the ambipolar diffusion model and the orbit motion limited approximation for the fine particle charging.

B. Effect of the plasma density gradient

Figure 2 shows the dependence of nondimensional ion velocity v_{iD}/V_{Ti} [Fig. 2(a)], microscopic ion current on the particle surface I_i/I_{i0} [Fig. 2(b)], and equilibrium nanoparticle charge Z_d/Z_{d0} [Fig. 2(c)] in three different discharge areas on the interelectrode distance L, where $I_{i0}=I_i(v_{iD}=0)$ and $Z_{d0}=Z_d(v_{iD}=0)$. It is clearly seen that the deviations from the "ambipolar drift-free" values are the largest in the area 3 in the vicinity of the electrode. Indeed, according to Eqs. (6)–(8) the ambipolar fluxes increase with the gradients of the electron and ion number densities, the latter being the largest in the near-electrode areas. One can see from Fig. 2(a) that at smaller interelectrode distances ($L<1$–3 cm) the directed "ambipolar" ion velocity v_{iD} exceeds the ion thermal speed by several times, up to one order of magnitude. When the space between the electrodes increases, the ratio v_{iD}/V_{Ti} decreases and becomes very small (<0.1) at $L>8$–10 cm. This reflects the relation of the ambipolar fluxes to the plasma nonuniformity.

On the other hand, one can notice that the microscopic ion currents are smaller than I_{i0}. Indeed, at larger distances between the electrodes, the effect of the directed ion current becomes weaker and the actual ion current computed by using Eq. (10) asymptotically approaches the value given by Eq. (1). Comparison of curves 1 and 3 in Fig. 2(b) shows that the deviation of the ion current from I_{i0} is larger in area 3, where the ion fluxes due to the plasma nonuniformity are more pronounced. In the low-interelectrode-gap case, when the directed ion velocities are much larger than V_{Ti} [see Fig. 2(a), $L<2$ cm], the "ion-wind" approximation (2) is accurate, with a reduced (down to $0.3I_{i0}$) microscopic ion current. The fact that the resulting ion current at $L\sim 10$ cm (curve 3) still remains approximately 15% lower than I_{i0} reflects the importance of the directed ion fluxes in the near-electrode (presheath) areas even at relatively large interelectrode distances. In the plasma bulk, the ion current reaches 96% of the ambipolar flux-free value at much smaller ($\sim$4 cm) distances between the electrodes.

The equilibrium nanoparticle charge prominently shows quite different behavior at smaller and larger interelectrode gaps. As can be seen from Fig. 2(c), $|Z_d|$ decreases with increasing L for $L<0.8$ cm in the plasma bulk, $L<1.6$ cm in the area 2, and $L<2.8$ cm in the near-electrode area. Thereafter, the particle charge increases with increasing L and tends to level off when the distance between the electrodes is large enough ($L\sim$9–10 cm). Physically, when the gap is small, the actual ion currents [Fig. 2(b)] are lower than I_{i0}, which results in excessive negative charge [curve 3 in Fig. 2(c) at $L<1$ cm]. As the ion current increases, the negative charge on nanoparticles becomes smaller. When the interelectrode gap increases, the relative importance of the ambipolar fluxes diminishes, and Z_d tends to reach the "drift-free" values, which results in well-resolved minima in the dependence $Z_d/Z_{d0}(L)$ shown in Fig. 2(c).

We emphasize that the deviations of the ion mean velocity v_i, microscopic ion current I_i, and nanoparticle charge Z_d from their ambipolar field- and flux-unaffected values appear to be significant in all three areas of the discharge. However,

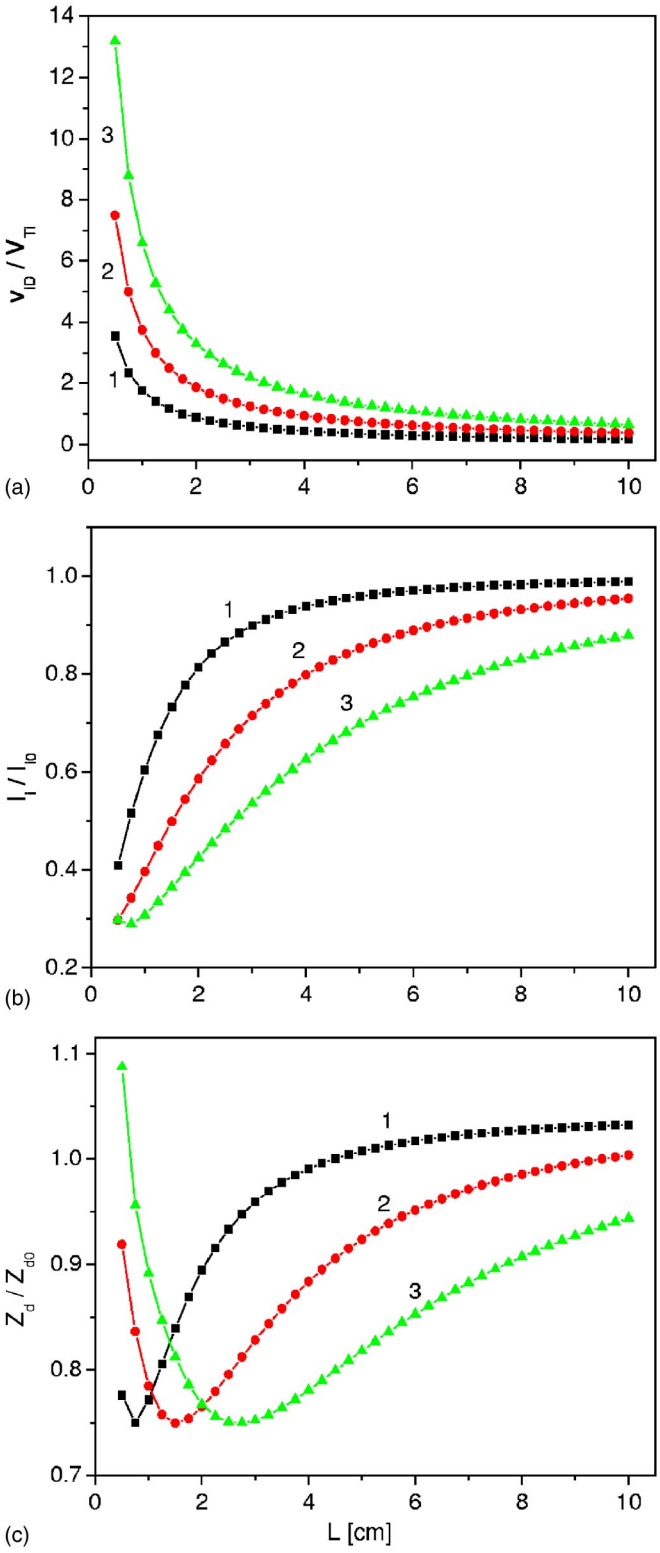

FIG. 2. (Color online) Dependence of nondimensional ion speed (a), ion charging current (b), and equilibrium fine particle charge (c) on the interelectrode spacing for the following set of plasma and particle parameters: $T_g=20$ °C, $p_0=5$ mTorr, $n_i(x=0)=8\times10^{10}$ cm^{-3}, $n_e(x=0)=6.4\times10^{10}$ cm^{-3}, $\sigma_{in}=3\times10^{-14}$ cm^2, $\sigma_{en}=5\times10^{-15}$ cm^2, $a_p=50$ nm, $T_e=2.5$ eV, and $T_i=0.1$ eV. Curves 1–3 correspond to the nanoparticle locations $0.55(L/2)$ (area 1 in Fig. 1), $0.75(L/2)$ (area 2), and $0.95(L/2)$ (area 3), respectively.

they are the most pronounced in the near-electrode area 3 with the largest gradients of the electron and ion number densities. In this area, typical deviations of the ion velocity (up to ~12–13 times) and charging current (up to ~3 −3.5 times) become larger with narrowing of the interelectrode gap. However, as can be seen from Fig. 2(c), Z_d departs (up to 25%) from its ambipolar field-free value Z_d' when L is decreased from 10 to ~2.7 cm and reapproaches Z_d' at smaller interelectrode distances.

It is also notable that quite similar (to those shown in Fig. 2) dependences of v_{iD}/V_{Ti} and I_i/I_{i0}, on the interelectrode spacing persist within the parameter ranges shown in Table I and do not show any notable irregularities. However, Z_d/Z_{d0} shows quite irregular dependences on L depending on the fine particle size and the ratio T_e/T_i reflecting the plasma nonisothermality. A relevant example will be discussed in Sec. III D. Nonetheless, in most cases considered, the deviation of the nanoparticle (NP) equilibrium charge from its "ambipolar field-free" values is strongest when the interelectrode gap is reasonably small ($L \approx 2$–4 cm).

C. Effect of collisions

We now explore the effect of the electron- and ion-neutral collisions on the ambipolar fluxes and the equilibrium nanoparticle charge. For this purpose, the working gas pressure and the values of the collisional cross sections σ_{en} and σ_{in} have been varied in computations. The dependence of v_{iD}/V_{Ti}, I_i/I_{i0}, and Z_d/Z_{d0} on the gas pressure in the range 1–100 mTorr for two different sets of collisional cross sections and two values of the neutral gas temperature is shown in Fig. 3. From Fig. 3(a) one can note that the directed ion velocity decreases quickly within the pressure range 1–10 mTorr and more slowly thereafter. Apparently, higher values of the working gas pressure result in higher rates of ion-neutral collisions, which, in turn, leads to slower ion drift velocities according to $v_{iD} \propto 1/\nu_{in}$.

In the example shown in Fig. 3, v_{iD} becomes subthermal when the gas pressure exceeds 2–5 mTorr. In the pressure range above 20 mTorr, one has $v_{iD} \ll V_{Ti}$ [Fig. 3(a)]. Thus, one should expect that in this particular case the contribution of the ambipolar fluxes to the microscopic ion charging currents and the equilibrium value of the particle charge is small when $p_0 > 20$ mTorr. This is consistent with Figs. 3(b) and 3(c) revealing that I_i/I_{i0} and Z_d/Z_{d0} level off very close to unity when the pressure reaches 20–40 mTorr. In the pressure range below 20 mTorr, the directed ion velocity is superthermal, which results in a noticeable general decrease of the ion charging current [Fig. 3(b)] and absolute value of the nanoparticle's negative charge [Fig. 3(c)].

The sets of parameters corresponding to curves 1–4 were chosen to generate different collision rates. These are strongly affected by the actual values of the collision cross sections and gas feedstock temperature. For example, the working gas temperatures are higher for curves 2 and 4, and the cross section of the ion-neutral collisions is higher for curves 3 and 4. From Fig. 3(a), it is seen that the directed ion velocity is higher at higher working gas temperatures and smaller collisional cross sections. We recall that $v_{iD} \propto 1/\nu_{in}$

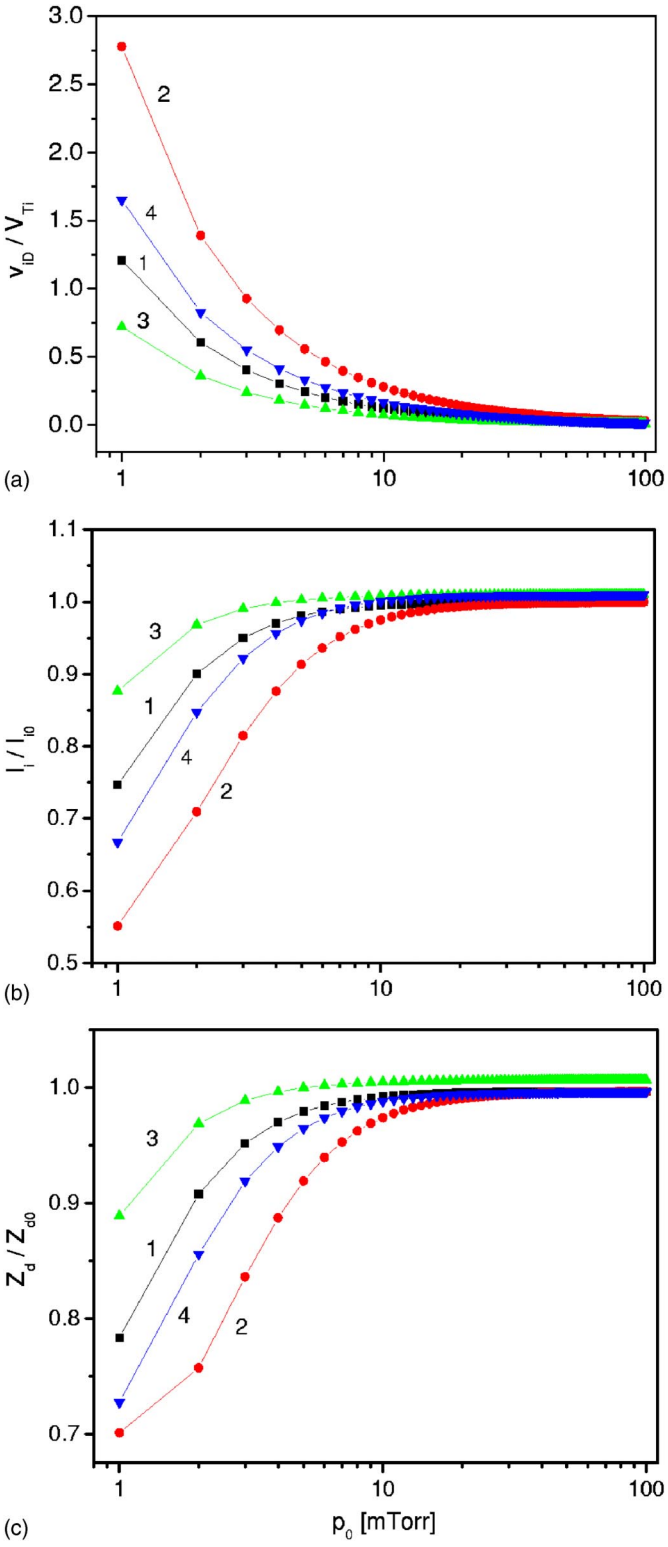

FIG. 3. (Color online) Same as in Fig. 2 as a function of the working gas pressure for the same nanoparticle position in area 3 and the following set of discharge and particle parameters: $L = 2$ cm, $n_i(x=0) = 6\times10^{10}$ cm^{-3}, $n_e(x=0) = 4.2\times10^{10}$ cm^{-3}, $a_p = 10$ nm, $T_e = 2.5$ eV, $T_i = 0.5$ eV, and $\sigma_{en} = 5\times10^{-15}$ cm^2. Curves 1 and 2 correspond to $\sigma_{in} = 3\times10^{-14}$ cm^2 and curves 3 and 4 to $\sigma_{in} = 5\times10^{-14}$ cm^2, respectively. Gas temperature is $T_g = 20$ °C in curves 1 and 3, and $T_g = 400$ °C in curves 2 and 4.

$\propto 1/N_n\sigma_{in}$. At a fixed gas pressure, assuming that $p_0 = N_n k_B T_g$, where T_g is the neutral gas temperature and k_B is the Boltzmann's constant, one has $v_{iD} \propto T_g/\sigma_{in}$. Comparing curves 2 and 4 with 1 and 3 in Fig. 3(a), we have $v_{iD}/V_{Ti}(T_g = 400\ °C) > v_{iD}/V_{Ti}(T_g = 20\ °C)$. Likewise, comparing curves 1 with 3 and 2 with 4 in the same figure, one concludes that $v_{iD}/V_{Ti}(\sigma_{in} = 3\times 10^{-14}\ \text{cm}^{-3}) > v_{iD}/V_{Ti}(\sigma_{in} = 5\times 10^{-14}\ \text{cm}^{-3})$. The changes in the microscopic ion current and, hence, the nanoparticle charge happen accordingly [Figs. 3(b) and 3(c)]. Specifically, $Z_d/Z_{d0}(T_g = 400\ °C) < Z_d/Z_{d0}(T_g = 20\ °C)$ and $Z_d/Z_{d0}(\sigma_{in} = 3\times 10^{-14}\ \text{cm}^{-3}) < Z_d/Z_{d0}(\sigma_{in} = 5\times 10^{-14}\ \text{cm}^{-3})$, with a similar tendency for the ratio I_i/I_{i0}. For the rates of the ion-neutral collisions $\nu_{in}^{(j)}$, where the superscript "j" is the same as the curve number in Fig. 3, we obtain $\nu_{in}^{(2)} < \nu_{in}^{(4)}$, $\nu_{in}^{(1)} < \nu_{in}^{(3)}$, $\nu_{in}^{(2)} < \nu_{in}^{(1)}$, and $\nu_{in}^{(4)} < \nu_{in}^{(3)}$, which explains the numerical results of Fig. 3.

At the end of this subsection, we remark that the deviations of the ion flux velocity and current and NP charge from their ambipolar flux-unaffected values show dependences on the gas feedstock pressure, temperature, and collision rates quite similar to Fig. 3 within the parameter ranges shown in Table I. Slightly nonmonotonic dependences of Z_d/Z_{d0} on p_0, T_g, and σ_{in} have been found for larger particles and lower values of the ratio T_e/T_i. Furthermore, the effect of variation of the electron-neutral collision cross section appears to be weak. For example, reduction of σ_{en} from $5\times 10^{-15}\ \text{cm}^2$ (value used in Fig. 3) to $1.5\times 10^{-15}\ \text{cm}^2$ results in changes in v_{Di}/V_{Ti}, I_i/I_{i0}, and Z_d/Z_{d0} not exceeding 1%. This is expected, as the electron charging current is predominantly thermal. Thus, Fig. 3 quantitatively reflects the effect of collisions on the NP charging in a broader parameter range. In all cases, the effect of ambipolar fluxes is weak at higher pressures, when the velocities of directed ion flows diminish due to stronger collisions.

D. Effect of the plasma nonisothermality

The nonisothermality of the plasma (usually represented by the ratio of the electron and ion temparatures T_e/T_i) is expected to play a prominent role in the nanoparticle charging process. To illustrate this effect, we have computed the nondimensional directed ion velocity [Fig. 4(a)], microscopic ion current [Fig. 4(b)], and nanoparticle charge [Fig. 4(c)] as a function of the electron temperature under different ion temperatures and charge imbalance in the plasma.

From Fig. 4(a) one can conclude that the ion velocities are in most cases superthermal. This is the case for either room-temperature ($T_i \sim 0.027$ eV, curves 1 and 3) or higher-temperature ($T_i \sim 0.3$ eV, curves 2 and 4) plasma ions. However, the ion flux is subthermal at $T_i \sim 0.3$ eV and electron temperatures below 1.7–1.9 eV [Fig. 4(a)]. Accordingly, the normalized ion currents are higher at $T_i \sim 0.3$ eV [Fig. 4(b), curves 2 and 4] than at $T_i \sim 0.027$ eV (curves 1 and 3). It is interesting to note that I_i/I_{i0} diminishes with T_e a bit more steeply in the case of the room-temperature ions.

Meanwhile, the deviations of the nanoparticle charge from its ambipolar flux-unaffected values depend quite differently on T_e at different ion temperatures. As can be seen from Fig. 4(c), Z_d/Z_{d0} increases (curves 1 and 3) and de-

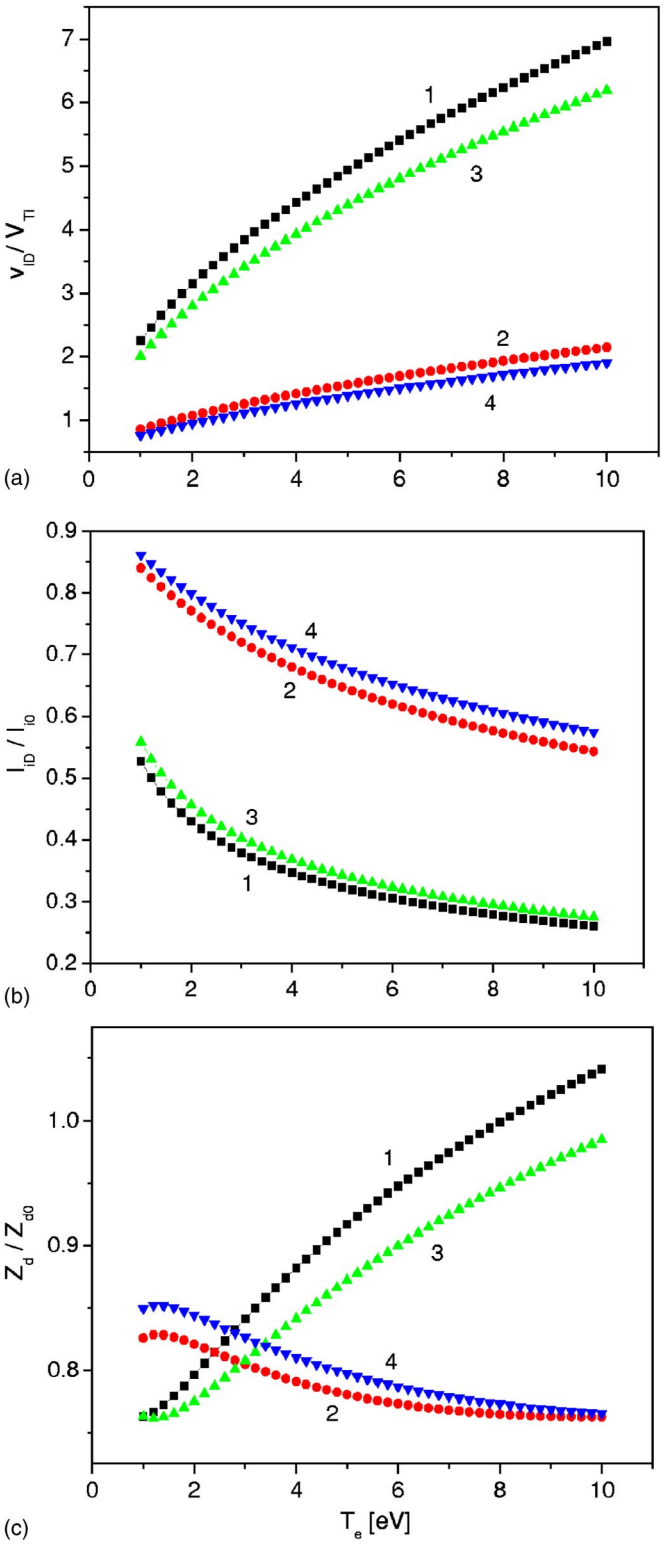

FIG. 4. (Color online) Same as in Fig. 2 as a function of the electron temperature for the same nanoparticle position in area 3 and the following set of discharge and particle parameters: $T_g = 50\ °C$, $L = 2$ cm, $p_0 = 10$ mTorr, $n_i(x=0) = 5\times 10^{10}\ \text{cm}^{-3}$, $a_p = 10$ nm, $\sigma_{in} = 3\times 10^{-14}\ \text{cm}^2$, and $\sigma_{en} = 5\times 10^{-15}\ \text{cm}^2$. Curves 1 and 3 correspond to $T_i = 0.027$ eV, and curves 2 and 4 to $T_i = 0.3$ eV. Electron number density $n_e(x=0) = 3.75\times 10^{10}\ \text{cm}^{-3}$ in curves 1 and 2 and $4.75\times 10^{10}\ \text{cm}^{-3}$ in curves 3 and 4.

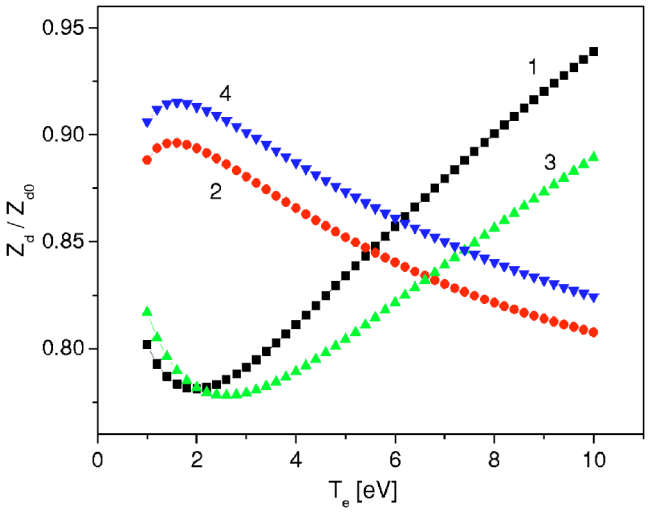

FIG. 5. (Color online) Same as in Fig. 4(c) for NP size and electron and ion densities ten times higher than in Fig. 4(c).

creases (curves 2 and 4) with T_e at T_i=0.027 and 0.3 eV, respectively. For larger particles, this dependence can become nonmonotonic in dense plasmas. For example, the normalized equilibrium charge of a 100-nm-sized particle in dense (with n_e and n_i one order of magnitude higher than in Fig. 4) plasmas decreases (curves 1 and 3) and increases (curves 2 and 4) at lower electron temperatures, as can be seen in Fig. 5. When the electron temperature reaches approximately 2–2.5 eV (T_i=0.027 eV) and 1.5–1.6 eV (T_i =0.3 eV), the tendency reverses. Presumably, this difference is related to different decline rates of the ion current at different ion temperatures and nonmonotonic variation of the electron current (9) in the range of electron temperatures considered (T_e=1–10 eV).

Different parameters for curves 1–4 [ion temperatures for curves (1,3) and (2,4) and imbalance between the electron and ion number densities for curves (1,2) and (3,4)] in Figs. 4 and 5 have been chosen to generate different values of the Bohm (ion-acoustic) velocity

$$V_B = \left(\frac{T_e}{m_i} \frac{n_{iS}}{n_{eS}} \right)^{1/2},$$

which is the speed the plasma ions gain on entering the near-electrode sheath of complex plasmas with unequal electron n_{eS} and ion n_{iS} number densities at the sheath edge [28]. In fine-particle-loaded plasmas this parameter is higher than in pristine plasmas since $n_{iS} > n_{eS}$. In our case, higher values of the Bohm velocity under the same interelectrode spacing and other parameters mean faster gains of the ion speed in the ambipolar flow. Thus, stronger plasma nonisothermality (larger ratios T_e/T_i), and charge imbalances (larger n_i/n_e) ensure higher V_B. From Fig. 4, one can deduce that the values of the Bohm velocity are higher for curves 1 and 3 compared to 2 and 4 due to larger ratios of the electron and ion temperatures. On the other hand, $(n_i/n_e)_{(1)} > (n_i/n_e)_{(3)}$, $(n_i/n_e)_{(2)} > (n_i/n_e)_{(4)}$, which means that the effect of ambipolar fluxes is stronger in the cases shown in curves 1 and 2 compared to 3 and 4, respectively. As can be seen from Fig. 4(b), higher values of the Bohm velocity at the plasma edges correspond to lower microscopic ion charging currents compared to the ambipolar flux-free (purely thermal) case. It is worthwhile to note that nonmonotonic variations of Z_d/Z_{d0} with T_e at different ion densities for larger particles suggest that the value of the nanoparticle charge is case sensitive and should be computed in each particular experiment by using the self-consistent set of the plasma and process parameters.

IV. DISCUSSION

In the above, we have considered the effect of ambipolar fluxes on the charging process of nanoparticles in a parallel-plate low-pressure discharge. The ambipolar flux originates due to intrinsic nonuniformities of the plasma glow sustained between the two parallel electrodes. Thus, even in the plasma bulk, where the nonuniformity is relatively weak, the directed ion flux often makes a significant contribution to the microscopic ion current that balances the electron charging current and determines the equilibrium nanoparticle charge. The electron current is weakly affected by the ambipolar flux since $v_{iD} \ll V_{Te}$. Thus, I_e is essentially a spherically symmetric thermal current. However, the directed ion fluxes can be either subthermal or superthermal depending on the interelectrode spacing, gas pressure, neutral gas temperature, collisional cross sections, electron and ion temperatures, and other parameters. When $v_{iD} \ll V_{Ti}$, the ion flux on the particle surface is almost spherically symmetric and it is fairly accurate to use Eq. (1) to calculate $|Z_d|$. This situation happens when the interelectrode spacing is large (and hence the plasma density gradients are small) or ion-neutral collision rates are reasonably high (which happens in the case considered when the gas pressure exceeds a few tens of mTorr). When the working gas pressure is low (below 5 mTorr in the case considered) and/or the gap between the electrodes is small (1–1.5 cm), one can use the "ion-wind" approximation (2) for the (almost unidirectional) ion current.

However, it turns out that both situations described by either Eq. (1) or Eq. (2) happen only in certain parameter ranges, and, generally speaking, the actual ion flux is neither spherically symmetric and purely thermal nor unidirectional and strongly superthermal. In the low-pressure case, which is very important for numerous plasma processing applications, the directed ion velocity is of the same order of magnitude as the ion thermal speed. In this case it is essential to use the general expression for the microscopic ion charging current (10), which is valid in the intermediate case when $v_{iD} \sim V_{Ti}$. As the results shown in Figs. 2–5 suggest, the discrepancy in the values of the equilibrium nanoparticle charge computed by using different approximations for the ion charging current can reach a couple of tens of percent.

We now discuss the implications of the above discrepancy on the modeling of particulate-loaded discharges and nanoparticle manipulation in the plasma-enhanced chemical vapor deposition systems. As we have mentioned above, the contribution of ambipolar fluxes is the most important in the low-pressure range, which is the most desirable for use of the plasma-based systems as nanomanipulating and nanoassembly tools. For example, driving the fine particles by using the

plasma forces (such as the ion and neutral drag or long-range electrostatic forces) is one of the future approaches for precise plasma-based nanoparticle manipulation [6,7]. This process would include the stages of particle trapping, processing, transport, and stacking into the desired nanoassembly patterns. It is imperative to note that most of the forces on the powder particles in the plasma scale differently with a_p, which is usually directly proportional to the equilibrium nanoparticle charge [29].

For example, the electrostatic force F_E that repels the negatively charged particles from similarly charged deposition surfaces scales as a_p, and hence $F_E \propto |Z_d|$. As our results suggest, taking account of the ambipolar fluxes usually results in a reduction of the negative electric charge. Hence, the repelling electric force could be noticeably reduced by the ambipolar fluxes. On the other hand, the directed ion fluxes can substantially contribute to the ion drag force which usually moves the particles toward the electrode. More importantly, sufficient acceleration of the particles in the plasma bulk and/or presheath areas can enable the NP to overcome the near-surface repulsive electrostatic potential barrier and deposit on the growth surface during the discharge run [30]. This is highly relevant to recent experiments on the low-pressure $Ar+H_2+CH_4$ plasma-assisted low-temperature fabrication of various carbon-based nanostructures [31–33], where monodisperse distributions of NPs over nanostructured carbon surfaces were frequently observed. Extensive ongoing efforts are focused on controllable incorporation of the plasma-grown NPs into amorphous carbon matrix or diversion of the NPs from ordered arrays of single-crystalline carbon nanotip structures [34].

It is remarkable that the effect of the ambipolar fluxes on the nanoparticle manipulation is twofold. First, the enhanced directed ion fluxes reduce the absolute value of the negative charge on the particle, which effectively lowers the near-surface repulsive electrostatic barrier. On the other hand, the additional ion wind drags the nanoparticles toward the surface, which is yet another factor that facilitates the successful deposition of the building units on the nanostructured surface.

If the charge proportion residing on fine particles is high enough (e.g. comparable with the charge densities of electrons and ions), the solid particle component can notably affect the discharge stability and performance. The accurate account for the directed ion fluxes would enable one to correctly estimate the quantity $n_p|Z_d|$ and describe the dynamics of the plasma species creation and loss, which is an essential component of self-consistent gas discharge modeling. Furthermore, the ambipolar fluxes affect the loss of the plasma species to the solid particles, which results in readjustment of the electron and ion sources, such as electron impact and Penning ionization, dissociation, secondary electron emission, etc. It is thus very likely that the electron energy distrubutions can be reshaped, which in turn can lead to changes in the effective electron temperature [35]. Above all, the ambipolar field (8) should be accurately included in the computation of the nonuniform electrostatic potential in the discharge. Some of these effects are a subject of our ongoing efforts and will be quantified in the near future.

The model presented is quite simple and sidesteps the details of the species creation and loss or power balance in the discharge. However, despite its apparent simplicity, the model is instrumental in revealing the effect of the ambipolar fluxes on the equilibrium nanoparticle charge and includes a minimum set of transport and collision parameters consistent with the accuracy of the results. For simplicity, a parallel-plate discharge in argon was considered. However, the model can be extended to other gases, including reactive gases such as silanes or hydrocarbons. To this end, the extension of the model toward other gases seems to be quite straightforward by using different values of the ion mass and collisional cross sections. The extension of the model toward more complex situations such as gas mixtures with charge exchange and other heavy particle collisions can be quite complicated. In this case, the main equations of the ambipolar model will need to be rederived to ensure the ambipolarity of the multi-ion flux. The inclusion of specific details of the particle and power balance and illustration of the effect of the ambipolar fluxes on nanoparticle charging (including sub-10-nm-sized nanoclusters, nanocrystallites, and powder aggregates) in specific discharge situations warrant forthcoming modeling efforts.

V. CONCLUSION

The above results indicate a possible vital role of the ambipolar fluxes in the charging of solid nanoparticles in parallel-plate glow discharges featuring nonuniform distributions of the electron and ion number densities. The relative importance of the directed ion fluxes is most pronounced when the interelectrode spacing is small and/or working gas pressures are low. In most cases, the directed ion velocity appears to be of the same order of magnitude as the ion thermal speed, which warrants the use of the general expression (10) for the microscopic ion charging currents [21]. It is notable that under certain conditions the ambipolar fluxes are appreciable even in the plasma bulk and should be properly accounted for in the modeling of various types of low-pressure gas discharges.

We emphasize that the purpose of this work is not a comprehensive discharge modeling. We have aimed, from a broader perspective, to pinpoint the importance of the ambipolar electric-field-driven ion fluxes in the nanoparticle charging in low-pressure gas discharge plasmas widely used for the synthesis and surface modification of advanced materials. The results are relevant to plasma-based nanoparticle manipulation and modeling of low-pressure low-temperature plasmas and should be tested in specific experimental situations.

ACKNOWLEDGMENTS

This work was supported by the Australian Research Council and the University of Sydney.

[1] G. S. Selwyn and E. F. Patterson, J. Vac. Sci. Technol. A **10**, 1053 (1992).
[2] P. Roca i Cabarrocas, J. Non-Cryst. Solids **266-269**, 31 (2000).
[3] *Nanotechnology Research Directions: Vision for Nanotechnology Research and Development in the Next Decade*, edited by M. C. Roco, S. Williams, and P. Alivisatos (Kluwer Academic, Amsterdam, 1999). See also U.S. National Nanotechnology Initiative, http://www.nano.gov
[4] L. Boufendi and A. Bouchoule, Plasma Sources Sci. Technol. **11**, A211 (2002).
[5] N. M. Hwang, J. Cryst. Growth **204**, 85 (1999).
[6] K. Ostrikov, Sing. J. Phys. **19**, 1 (2003).
[7] S. V. Vladimirov and K. Ostrikov, Phys. Rep. **393**, 175 (2003).
[8] E. Abdel-Fattah and H. Sugai, Appl. Phys. Lett. **83**, 1533 (2003).
[9] H. H. Hwang, E. R. Keiter, and M. J. Kushner, J. Vac. Sci. Technol. A **16**, 2454 (1998).
[10] K. Ostrikov, I. B. Denysenko, S. V. Vladimirov, S. Xu, H. Sugai, and M. Y. Yu, Phys. Rev. E **67**, 056408 (2003).
[11] I. B. Denysenko, S. Xu, M. Y. Yu, and C. H. Diong, J. Appl. Phys. **94**, 6097 (2003).
[12] K. De Bleecker, A. Bogaerts, R. Gijbels, and W. Goedheer, Phys. Rev. E **69**, 056409 (2004).
[13] L. Stenflo and M. Y. Yu, Phys. Plasmas **10**, 912 (2003).
[14] S. Amiranashvili, M. Y. Yu, and L. Stenflo, Phys. Rev. E **67**, 016408 (2003).
[15] S. Amiranashvili and M. Y. Yu, Phys. Plasmas **9**, 4825 (2002).
[16] J. X. Ma, M. Y. Yu, X. P. Liang, J. Zheng, W. D., and C. X. Yu, Phys. Plasmas **9**, 1584 (2002).
[17] M. S. Barnes, J. H. Keller, J. C. Forster, J. A. O'Neill, and D. K. Coultas, Phys. Rev. Lett. **68**, 313 (1992).
[18] J. Goree, Plasma Sources Sci. Technol. **3**, 400 (1994).
[19] A. Barkan, N. D'Angelo, and R. L. Merlino, Phys. Rev. Lett. **73**, 3093 (1994).
[20] The notion of "ambipolar fluxes" R. N. Franklin, J. Phys. D **36**, 826 (2003), rather than that of the "ambipolar diffusion" is used here to emphasize the presence of ambipolar electric fields in the plasma.
[21] E. C. Whipple, Rep. Prog. Phys. **44**, 1197 (1981).
[22] Here, we have adopted the term "nanoparticles" conventionally used for fine particles in this size range [see, e.g., M. J. Pitkethly, Nano Today **2** (12), 36 (2003)]. The lower size limit of 10 nm has been chosen due to the limitations of the particle charging theory used in the computations.
[23] K. N. Ostrikov, S. V. Vladimirov, M. Y. Yu, and G. E. Morfill, Phys. Rev. E **61**, 4315 (2000).
[24] K. N. Ostrikov, S. V. Vladimirov, M. Y. Yu, and G. E. Morfill, Phys. Plasmas **7**, 461 (2000).
[25] S. I. Popel, V. N. Tsytovich, and M. Y. Yu, Astrophys. Space Sci. **256**, 107 (1998).
[26] M. A. Lieberman and A. J. Lichtenberg, *Principles of Plasma Discharges and Materials Processing* (Wiley, New York, 1994).
[27] *Dusty Plasmas: Physics, Chemistry, and Technological Impacts in Plasma Processing*, edited by A. Bouchoule (Wiley, New York, 1999).
[28] K. N. Ostrikov and M. Y. Yu, IEEE Trans. Plasma Sci. **26**, 100 (1998).
[29] For spherical particles $|Z_d| \propto \Delta\phi_s C$, where $C \propto a$ is the particle's capacitance. However, the direct proportionality between the charge and size often fails for sufficiently small or large particles.
[30] P. P. Rutkevych, I. B. Denysenko, S. Xu, and R. Storer, Phys. Scr. **70**, 322 (2004); P. P. Rutkevych, K. Ostrikov, S. V. Vladimirov, and S. Xu, J. Appl. Phys. **96**, 4421 (2004).
[31] I. B. Denysenko, S. Xu, P. P. Rutkevych, J. D. Long, N. A. Azarenkov, and K. Ostrikov, J. Appl. Phys. **95**, 2713 (2004).
[32] Z. L. Tsakadze, K. Ostrikov, J. D. Long, and S. Xu, Diamond Relat. Mater. **13**, 1923 (2004).
[33] Z. L. Tsakadze, K. Ostrikov, and S. Xu, Surf. Coat. Technol. **191/1**, 49 (2004).
[34] K. Ostrikov, Z. Tsakadze, I. Denysenko, P. P. Rutkevych, J. D. Long, S. V. Vladimirov, and S. Xu (unpublished).
[35] H. Sugai, I. Ghanashev, M. Hosokawa, K. Mizuno, K. Nakamura, H. Toyoda, and K. Yamauchi, Plasma Sources Sci. Technol. **10**, 378 (2001).